

## Highlights

### **Increasing the skill of short-term wind speed ensemble forecasts combining forecasts and observations via a new dynamic calibration**

Gabriele Casciaro, Francesco Ferrari, Daniele Lagomarsino Oneto, Andrea Lira-Loarca, Andrea Mazzino

- First attempt to couple in an efficient and economic way real-time data and ensemble predictions.
- First assessment of the added value of real-time observations in a wind calibration.
- Real-time data can be easily and economically ingested in an EMOS-based calibration.
- Ingestion of real-time data produces noticeable benefits vs. static calibrations.
- Real-time data provide added value to the whole wind predictive probability density.

# Increasing the skill of short-term wind speed ensemble forecasts combining forecasts and observations via a new dynamic calibration

Gabriele Casciaro<sup>a</sup>, Francesco Ferrari<sup>a,b</sup>, Daniele Lagomarsino Oneto<sup>c,a</sup>,  
Andrea Lira-Loarca<sup>a</sup>, Andrea Mazzino<sup>a,b,\*</sup>

<sup>a</sup>*DICCA, Department of Civil, Chemical and Environmental Engineering. University of Genoa, Via Montallegro 1, Genoa, 16145, Genoa, Italy*

<sup>b</sup>*INFN, National Institute of Nuclear Physics, Genoa section, Via Dodecaneso 33, Genoa, 16146, Genoa, Italy*

<sup>c</sup>*MALGA, Machine Learning Genoa Center. University of Genoa, Via Dodecaneso 35, Genoa, 16146, Genoa, Italy*

---

## Abstract

All numerical weather prediction models used for the wind industry need to produce their forecasts starting from the main synoptic hours 00, 06, 12, and 18 UTC, once the analysis becomes available. The six-hour latency time between two consecutive model runs calls for strategies to fill the gap by providing new accurate predictions having, at least, hourly frequency. This is done to accommodate the request of frequent, accurate and fresh information from traders and system regulators to continuously adapt their work strategies. Here, we propose a strategy where quasi-real time observed wind speed and weather model predictions are combined by means of a novel Ensemble Model Output Statistics (EMOS) strategy. The success of our strategy is measured by comparisons against observed wind speed from SYNOP stations over Italy in the years 2018 and 2019.

*Keywords:*

---

\*Corresponding author

*Email addresses:* [gabriele.casciario@edu.unige.it](mailto:gabriele.casciario@edu.unige.it) (Gabriele Casciaro),  
[francesco.ferrari@edu.unige.it](mailto:francesco.ferrari@edu.unige.it) (Francesco Ferrari),  
[daniele.lagomarsino@edu.unige.it](mailto:daniele.lagomarsino@edu.unige.it) (Daniele Lagomarsino Oneto),  
[andrea.lira.loarca@unige.it](mailto:andrea.lira.loarca@unige.it) (Andrea Lira-Loarca), [andrea.mazzino@unige.it](mailto:andrea.mazzino@unige.it)  
(Andrea Mazzino)

wind forecasting, probabilistic forecasting, dynamic forecast calibration, ensemble model output statistics, wind forecast based on real-time conditions, Numerical Weather Prediction models

---

## 1. Introduction

Global cumulative installations of onshore and offshore wind are expected to exceed 1 TW before 2025 (Global Wind Energy Council, 2021). This means that the contribution of wind power in power systems is becoming increasingly important. The downside is that detailed schedule plans and reserve capacity must be properly set by power system regulators (Impram et al., 2020) facing the intrinsic problem of the highly intermittent nature of wind, making this very hard to predict. The accuracy of wind forecasts thus becomes an issue of paramount importance for the wind industry.

In a recent work by Casciaro et al. (2021), a novel accurate Ensemble Model Output Statistics (EMOS) strategy for calibrating wind speed/power forecasts from an Ensemble Prediction System (EPS) has been proposed and its superiority when compared against more parsimonious strategies in the 0-48 h look-ahead forecast horizon clearly emerged. However, because all global weather models start their run from analysis corresponding to the main synoptic hours 00, 06, 12, and 18 UTC, weather predictions (of any forecast horizons) necessarily remain frozen for six hours. This limitation is in sharp contrast with the needs of power system regulators, as well as of traders for marketing wind energy, who need to adapt their strategies hour after hour in a quasi-continuous way. It is thus very important to propose accurate strategies which give fresh information on the wind speed in a given location continuously evolving between two consecutive main synoptic hours. Proposing a strategy with such characteristics is the main aim of the present paper. In plain words, we propose a novel, parsimonious, dynamic EMOS strategy where the parameters entering the EMOS predictive probability density function now also depends on real-time (or quasi-real time) observed wind speed data. Our strategy combines two well-known advantages for wind prediction by physical methods (i.e. based on numerical weather prediction, NWP, models) and statistical methods (i.e. statistical models based on time-series of past measured observables and/or observation-driven machine-learning (ML) based methods). While the former methods are suitable for predicting wind (and, more generally, any meteorological observable) in the forecast horizon larger than, say, 6 hours, the latter strategies turn out to have greater

skills for short-term forecasting, say, less than a few hours ahead. For a review of those methods and discussions of their skills, see, e.g., Soman et al. (2010) and the references therein. We will show that combining quasi real-time observed data and predictions via a suitable EMOS strategy provides an optimal assembly strategy which outperforms the single aforementioned strategies when acting separately. This turns out to be the case both in terms of point indices (the standard NMAE and correlation coefficient) and via suitable statistical indices to assess the whole probability density function of the (calibrated) ensemble forecast error.

For our dynamic strategy to be used operatively, the observed wind speed on the site of interest must be available in real/quasi-real time, other than as a record of past observations for implementing the static calibration.

The paper is organized as follows. In Sec. 2.1 we introduce the wind speed observations dataset used both to train our calibration algorithm and for its testing. Sec. 2.2 presents the forecast data from the Ensemble Prediction System (EPS) of the ECMWF. Sec. 3.1 provides a quick review of the standard Ensemble Model Output Statistics (EMOS). A very recent generalization of standard EMOS to account for nonlinearities is described in Sec. 3.2. The algorithm we propose to ingest real-time observed data in a EMOS strategy is described in Sec. 4.1. The new algorithm is tested in different respects in Secs. 4.2 and 4.3. The final section is devoted to draw some conclusions and perspectives.

## 2. Wind data

### 2.1. Observed data from SYNOP stations

From 2018 to 2019, SYNOP meteorological data were collected at 42 locations across Italy. According to ICAO specifications, the SYNOP anemometers record wind speed (knots) as an average over 10 minutes at a nominal measurement height of 10 meters a.g.l. (ICAO, 2007) with hourly frequency. The stations are arranged fairly uniformly across the peninsula, as shown in Figure 1. Data have been split using 2018 as training set and 2019 as test set.

### 2.2. Forecast data from the ECMWF Ensemble Prediction System (EPS)

The Ensemble Prediction System (EPS) from the European Centre for medium-range weather forecasts (ECMWF), is made up of 51 members: a control forecast with no perturbations and 50 forecasts created by adding



Figure 1: Location of a selected group of Italian SYNOP stations used in the present study for forecast calibration and testing. Colors are coded according to the orography elevation.

small perturbations to the best-known initial condition, using a mathematical formulation based on singular vector decomposition and stochastic parameterization to represent model uncertainties (Buizza, 1995; Leutbecher and Palmer, 2008).

The EPS used in this study has spectral triangular truncation with a cubicoctahedral grid Tco639 and 91 layers with a top of atmosphere pressure of 0.01 hPa (Buizza, 2018) and a resolution of about 18 km (Persson, 2001).

Although four runs per day are made available from the ECMWF, in the present study the sole EPS runs starting from the 00 UTC analysis have been considered in the first 48-hour look-ahead forecast horizon.

Although there are robust evidences (Molteni et al., 1996; Montani et al., 2019) that observed mean and variance correlate well with the EPS ensemble mean and variance, all EPS members frequently underestimate and are underdispersive with respect to observations. Then EPS forecasts must be properly calibrated, especially for close-to-surface meteorological data. The surface wind speed is just a relevant example considered in the present paper.

### 3. The static calibration strategy

We provide in this section a brief review of the so-called Ensemble Model Output Statistics (EMOS) through which a raw ensemble forecast can be accurately transformed into a predictive probability density function, with a simultaneous correction for biases (additive and multiplicative) and dispersion errors (Gneiting et al., 2005; Thorarinsdottir and Gneiting, 2010). A generalization recently proposed by Casciaro et al. (2021) accounting for nonlinear relationships between predictands and both predictors, and other weather observables used as conditioning variables will be also reviewed. Both strategies share the common feature of being static, meaning that they do not exploit real-time (or quasi-real time) observed data.

#### 3.1. The standard Ensemble Model Output Statistics

The standard EMOS strategy, here denoted as EMOS<sub>0</sub>, is a generalization of multiple linear regressions, also known as Model Output Statistics (MOS) (Glahn and Lowry, 1972), which is commonly used to calibrate deterministic forecasts.

Let us consider  $M$  ensemble member forecasts,  $X_1, \dots, X_M$ , of a univariate continuous, positive-defined variable  $Y$ , the meteorological observable of interest, here the wind speed in one specific location and given look-ahead forecast time.

The EMOS method uses a parametric distribution of the following general form:

$$Y \mid X_1, \dots, X_M \sim f(Y \mid X_1, \dots, X_M) \quad (1)$$

where the left-hand side denotes the fact that the distribution is conditional on the ensemble member forecasts.

Gneiting et al. (2006) proposed the truncated normal distribution (TN) as a model for the wind speed conditional distribution  $f$ . An alternative distribution, the log-normal (LN), has been proposed by Baran and Lerch (2015) even if the Authors found that the TN-LN mixture model outperforms the traditional TN. The gamma distribution was finally suggested by Scheuerer and Möller (2015). All these options, and other variants, have been extensively discussed and compared by Wilks (2018).

Among all possible choices, in the present study we selected the gamma distribution,  $\mathcal{G}(\mu, \sigma^2)$ , as recently exploited by Casciaro et al. (2021) with excellent results. This distribution is fully described by two parameters: the shape parameter  $k$  and the scale parameter  $\theta$ . Their expressions in terms of the mean  $\mu$  and variance  $\sigma^2$  read:  $k = \mu^2/\sigma^2$  and  $\theta = \sigma^2/\mu$  with  $\mu$  and  $\sigma^2$  given by:

$$\mu = a + b_1 X_1 + \dots + b_M X_M \quad (2)$$

$$\sigma^2 = c + d S^2. \quad (3)$$

The coefficients  $a, b_1, \dots, b_M, c, d$  are non-negative parameters and  $S^2$  is the variance of the EPS, a quantitative measure of the ensemble spread.

Gneiting et al. (2005) proposed a strategy based on the minimization of the Continuous Ranked Probability Score (CRPS) to determine the EMOS<sub>0</sub> free parameters (Hersbach, 2000). In plain terms, the CRPS is defined as

$$CRPS(F, Y) = \int_{-\infty}^{\infty} [F(x) - H(x - Y)]^2 dx \quad (4)$$

where  $F$  is the cumulative probability function associated to the gamma density function  $\mathcal{G}$ ,  $Y$  is the observation, and  $H$  is the Heaviside function, which returns 0 when  $x < Y$  and 1 otherwise.

A closed form for the CRPS for the gamma distribution has been obtained by Scheuerer and Möller (2015) making the minimization procedure easy and fast. For an observation-forecast pair  $(Y, \mathbf{X})$  it reads:

$$crps = Y \left[ 2P \left( k, \frac{Y}{\theta} \right) - 1 \right] - k\theta \left[ 2P \left( k + 1, \frac{Y}{\theta} \right) - 1 \right] - \frac{\theta}{\beta \left( \frac{1}{2}, k \right)} \quad (5)$$

with  $Y$  being the observation,  $P$  the incomplete gamma function (Abramowitz and Stegun, 1948), and  $\beta$  the beta function. The forecast vector  $\mathbf{X} = (X_1, \dots, X_M)$  comes into the expression (5) via the parameters  $k$  and  $\theta$ .

The quantity to be minimized in a training set where both observations and forecasts are available is:

$$CRPS = \frac{1}{N} \sum_{i=1}^N crps(\mathbf{X}_i, Y_i) \quad (6)$$

with  $i$  denoting the  $i$ -th observation-forecast pair and  $N$  is the total number of pairs in the training set, here corresponding to the whole year 2018..

The CRPS combines calibration and informativeness in one index, thus allowing the evaluation of predictive performance that is based on the paradigm of maximizing the sharpness of the predictive distributions subject to calibration (Gneiting et al., 2007).

### *3.2. Accounting for non-linearities and small-scale dynamic effects: an evolution of the standard EMOS strategy*

Very recently (Casciaro et al., 2021) proposed a novel EMOS strategy and tested it against field measurements. The new strategy turned out to be largely superior with respect to the standard EMOS. The main strengths of the approach, baptized EMOS<sub>+4r</sub> by Casciaro et al. (2021), is that nonlinear features can be easily and economically accounted by conditioning meteorological variables. The strategy also deals with the issue related to the model grid-point best representing weather conditions observed at the ground station. This issue, particularly severe in regions having relevant small-scale orographic variations, arises one to the coarse spatial resolution of the EPS (as well as of any general circulation model).

To summarize the main idea of the method, let us consider  $X_i^j$  the  $i$ -th ensemble member forecast on the  $j$ -th model grid-point ( $j = 1, \dots, 4$  spans over the nearest model grid-points to the ground station) and  $S^{2j}$  the members variance on the  $j$ -th model grid-point. We also denote by  $Z_1, \dots, Z_q$  the  $q$  categorical variables (e.g., the wind direction, the hour of the day, the height of the boundary layer, among others reported by Casciaro et al. (2021)) expected to be useful to disentangle the EPS forecast error.

The EMOS<sub>+4r</sub> predictive distribution is exactly as in the standard EMOS<sub>0</sub> apart the key fact that now the free parameters are best-fitted for each combination of classes' levels, via a training set, by minimizing the CRPS.

In plain terms, mean and variance of the predictive distribution are now



given by:

$$\mu = a(Z_1, \dots, Z_q) + \sum_{i=1, j=1}^{M, 4} b_{ij}(Z_1, \dots, Z_q) X_i^j \quad (7)$$

$$\sigma^2 = c(Z_1, \dots, Z_q) + \sum_{j=1}^4 d_j(Z_1, \dots, Z_q) S^{2j} \quad (8)$$

where  $j$  spans over the 4 model grid points around the station.

The last step of the strategy is to perform a final EMOS<sub>0</sub> downstream of previous calibration steps with the aim of allowing a synchronization of the forecast to the current climate trend. This aim is achieved in terms of a rolling training over the past 40 days without conditioning.

#### 4. The dynamic calibration

The main strengths of the EMOS<sub>+4r</sub> strategy can be summarized as follow: i) it accounts for nonlinear dependencies between predictands and both predictors and other weather observables used as conditioning variables; ii) it deals with the issue of the model grid-point selection best representing the weather at the ground station; iii) it allows the calibrated forecast to be aligned with the current weather climate via a rolling training.

These remarkable strengths are accompanied by the weak point of being unable to ingest real-time weather information. These these could be used latter on to extrapolate ahead in time the model error which can be quantified at the present time if observations are made available outside of the synoptic hours. Once the model error is extrapolated to the future via some suitable data-driven statistical methods, it can be exploited to further correct forecast error in the nearest future. How much the correction will be effective far from the hour at which the real-time observation is available is an issue to be addressed in the following sections.

##### 4.1. The proposed algorithm

This section illustrates how the potential benefit of real-time observations can be optimally integrated with the EMOS<sub>+4r</sub> strategy giving birth to a new dynamic calibration strategy which will be also tested against different alternative approaches.

In order to ensure greater clarity and better understanding, we report in Figure 2 the kernel of the calibration, i.e. a general EMOS having N input

predictors for the ensemble mean,  $K$  input predictors for the ensemble variance, and  $q$  conditioning variables. The values of  $N$ ,  $q$ , and  $K$  will vary from case to case in the different steps of the calibration we will show in the following. The first step (here denoted by Step 0) is to apply the EMOS kernel to

**EMOS**

$$\mu = a(\mathbf{Z}) + \sum_{i=1}^N b_i(\mathbf{Z}) X_i$$

$$\sigma^2 = c(\mathbf{Z}) + \sum_{j=1}^K d_j(\mathbf{Z}) S_j^2$$

$X_i$ : i-th of  $\mathbf{X}$

$S_j$ : j-th of  $\mathbf{S}$

Figure 2: Schematic view of the EMOS kernel of the dynamic calibration:  $\mathbf{Z} = (Z_1, \dots, Z_q)$  are  $q$  categorical conditioning variables entering in the model parameters  $a, b, c$ , and  $d$ ;  $\mathbf{X} = (X_1, \dots, X_N)$  are  $N$  input predictors for the mean,  $\mu$ , of the EMOS predictive distribution;  $\mathbf{S} = (S_1, \dots, S_K)$  are  $K$  input predictors for the variance,  $\sigma$ , of the EMOS predictive distribution.

each of the 4 nearest model grid-points to the SYNOP station without using conditioning variables. This step is schematically depicted in Figure 3 for a representative model grid-point. By applying it to each of the four model

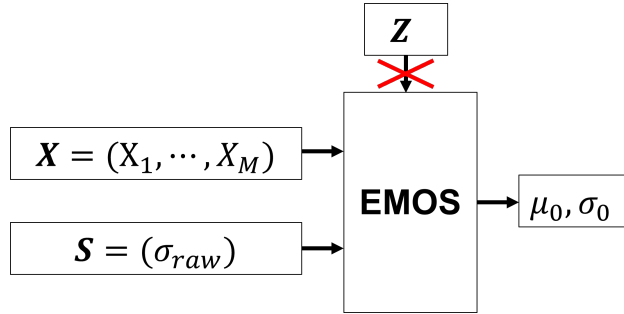


Figure 3: Schematic representation of the Step 0 of our dynamic calibration in one of the 4 nearest model grid-points to a station. Input:  $\mathbf{X} = (X_1, \dots, X_M)$  are the  $M$  members of the ensemble forecasts;  $\mathbf{S} = (\sigma_{raw})$  is the square root of the variance of the ensemble member forecasts ( $K=1$ ). Output:  $\mu_0$  and  $\sigma_0$  the parameters of the calibrated predictive distribution.

grid-points, we end up with  $\mu_0^1, \dots, \mu_0^4; \sigma_0^1, \dots, \sigma_0^4$ , with the upper indices being associate to the model grid-point among the four nearest to the ground station. The purpose of this first step is simply to reduce the forecast BIAS

while maintaining unchanged the correlation between forecasts and observations. The resulting calibrated parameters from Step 0 are used as input to the second step of our calibration, Step 1.

New players ( $O_1, \dots, O_P$ ) come into Step 1 and involve  $P$  observed data available at a reference hour, say  $h$  (i.e.  $h$  is the last hour at which observed data are available and usable). In way of example,  $P = 2$  with  $O_1$  being the persistence built from the wind speed known at hour  $h$ , and  $O_2$  is the diurnal-cycle-based persistence, i.e. a forecast built in terms of the observations occurred in the past 24 hours. Figure 4 summarizes how observations are combined with the results from Step 0 carried out for the four closest-to-the-station model grid-points. From Step 1 we end up with the parameters

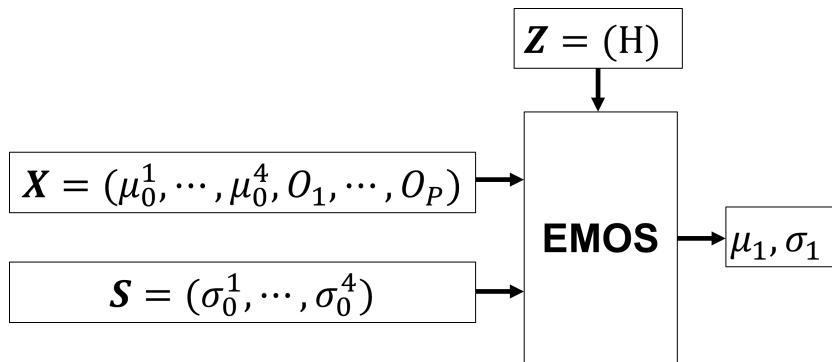


Figure 4: Schematic representation of Step 1 of our dynamic calibration involving the information coming from Step 0. Input:  $\mathbf{X} = (\mu_0^1, \dots, \mu_0^4, O_1, \dots, O_P)$ , where  $\mu_0^1, \dots, \mu_0^4$  come from Step 0 iterated for the four closest-to-the-station model grid-points, and  $(O_1, \dots, O_P)$  are  $P$  variables related to station observations available at hour  $h$ ;  $\mathbf{S} = (\sigma_0^1, \dots, \sigma_0^4)$  comes from Step 0. Conditioning variables:  $\mathbf{Z} = (H)$  is the hour of the day (hourly step within the 24 hours). Output:  $\mu_1$  and  $\sigma_1$  the calibrated parameters of the Step 1 predictive distribution.

$\mu_1, \sigma_1$  of the predictive distribution. This latter now becomes a function not only of the ensemble members but also of suitable observations.

Having used the hour of the day as conditioning variables, the information on how far one is from the last available observation (at hour  $h$ ) indirectly comes into the model.

We now need to join all previous steps in terms of suitable conditioning variables. This is the Step 2 of our calibration as summarized in Fig. 5. The result of this last step of calibration is the calibrated predictive probability gamma function,  $\mathcal{G}(\mu_2, \sigma_2)$ , which selects the best model grid-point

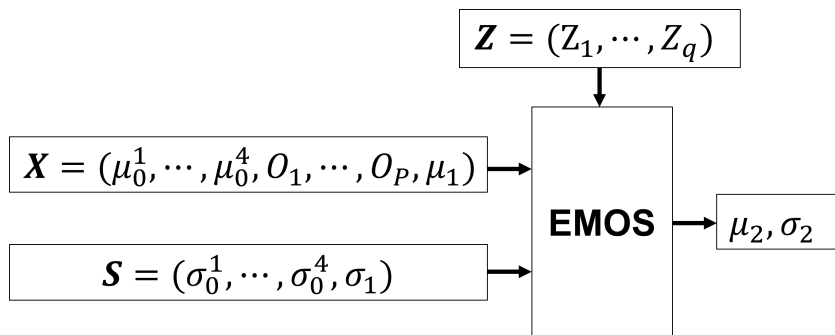


Figure 5: Schematic representation of Step 2 of our dynamic calibration. Input:  $\mathbf{X} = (\mu_0^1, \dots, \mu_0^4, O_1, \dots, O_P, \mu_1)$  where  $\mu_0^i$  ( $i = 1, \dots, 4$ ) comes from Step 0,  $(O_1, \dots, O_P)$  are  $P$  station observations available at hour  $h$ ;  $\mu_1$  comes from Step 1;  $\mathbf{S} = (\sigma_0^1, \dots, \sigma_0^4, \sigma_1)$  where  $\sigma_0^i$  comes from Step 0,  $\sigma_1$  comes from Step 1. Conditioning variables:  $\mathbf{Z} = (Z_1, \dots, Z_q)$ , selected following the same procedure as in Casciaro et al. (2021). Output:  $\mu_2$  and  $\sigma_2$ , the Step 2 calibrated parameters of the predictive gamma distribution.

performance, disentangles the model error in terms of suitable conditioning variables and, finally, synchronizes the forecast with the most recent observed wind speed at the station. We however found (see Sec. 4.2 for a quantitative analysis) that one more step is needed in order to extend ahead in time as much as possible the benefit of real-time observations. This final step (Step 3) is sketched in Figure 6. It simply joins the static calibration  $\text{EMOS}_{+4r}$  by Casciaro et al. (2021), with parameters  $\mu_s, \sigma_s$ , (where the subscript 's' is meant to stress out that such parameters are from a 'static' calibration) with those coming from Step 2. The final result is the gamma probability density function,  $\mathcal{G}(\mu_d, \sigma_d)$ , with  $\mu_d$  and  $\sigma_d$  coming from Step 3 of Fig. 6.

#### 4.2. Quantifying the importance of the different steps of calibration

Let us start to quantify the added value brought by single steps of our dynamic calibration by assuming that observed data are available at  $h = 9$  UTC. Here  $P = 1$  and  $O_1$  is the persistence built from the wind speed known at hour  $h$ . In order to quantify the benefit brought by Step 0 of our calibration, we compare in Fig. 7 the results of our dynamic calibration obtained with and without Step 0, respectively. This is done in terms of the skill score (see Appendix A) where the skill of the calibrated forecast from the complete calibration (i.e. starting from Step 0) is comparatively quantified against the calibrated forecast from the dynamic calibration now

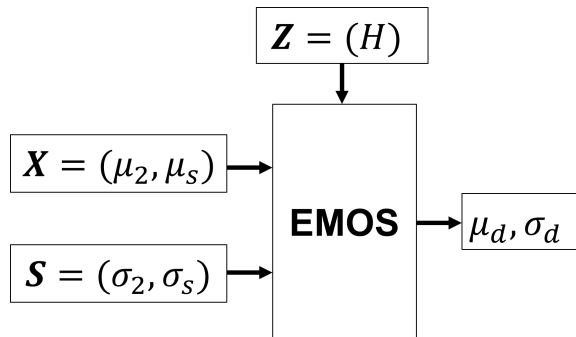


Figure 6: Schematic representation of Step 3, the last step of our dynamic calibration. Input:  $\mathbf{X} = (\mu_2, \mu_s)$  and  $\mathbf{S} = (\sigma_2, \sigma_s)$  where  $\mu_s$  and  $\sigma_s$  come from the  $EMOS_{+4r}$  static calibration by Casciaro et al. (2021) and reviewed in Sec. 3.2. The parameters  $\mu_2$  and  $\sigma_2$  come from Step 2 of our calibration. Conditioning variables:  $\mathbf{Z} = (H)$  as in Fig. 4. Output:  $\mu_d$  and  $\sigma_d$  the parameters of the final calibrated gamma predictive probability density function.

starting directly from Step 1 using the  $EMOS_{+4r}$  mean and variance as input. As one can see from the figure, apart the first hour of forecast, there is a clear added value brought by Step 0, as quantified both in terms of the NMAE index and in terms of the correlation coefficient. In Fig. 8 the importance of Step 2 is quantified similarly to what we did in Fig. 7: for both the NMAE index and the correlation coefficient, the skill score of the complete dynamic calibration is computed taking the forecast calibrated from the dynamic calibration without Step 2 as a reference. The results from Fig. 8 clearly indicate the added value brought by Step 2, especially in the first 5 hours of forecast.

We conclude by quantifying the role of Step 3. This is done in Fig. 9 where the reference calibrated forecast is the one coming from the dynamic calibration now without using Step 3. Also in this case the importance of the selected Step 3 is evident.

#### 4.3. Assessing the dynamic calibration via statistical indices

Having justified the added value brought by single steps of our dynamic calibration, we now pass to assess the performances of the dynamic calibration against different forecasts, both static, based on calibrated forecast from NWP models, and statistical, built solely in terms of past observed data, using persistence (i.e. the simplest way to build a forecast from a given observation) and a ML-based prediction. Here we consider the simplest way

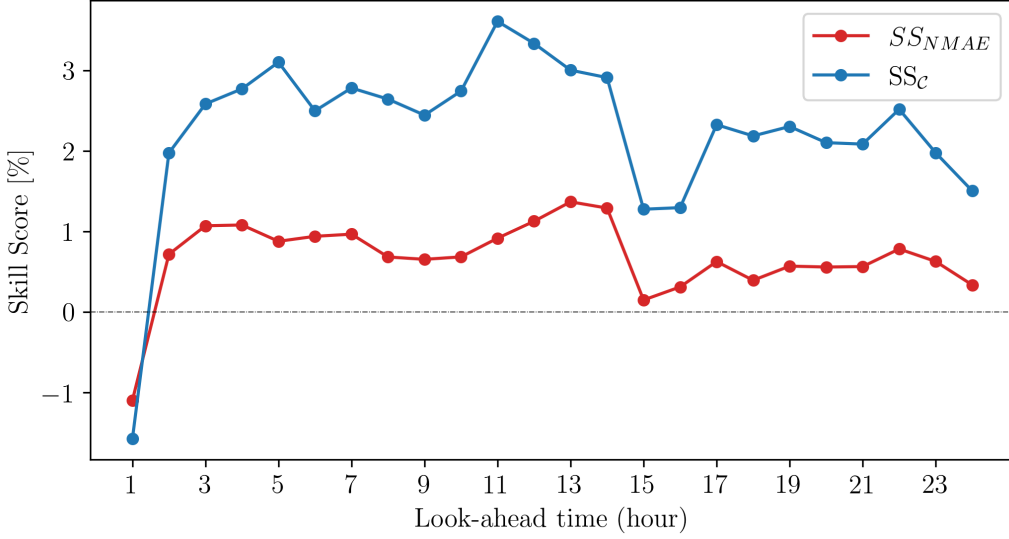


Figure 7: Mean skill score (of the skill scores computed at each station) for both the NMAE index and the correlation coefficient, as a function of the look-ahead time, for the complete dynamic calibration (i.e. the one starting from Step 0) where the observed data at  $h = 9$  UTC are used. The reference calibration against which the skill scores have been calculated is the same complete dynamic calibration which starts from Step 1 using the  $EMOS_{+4r}$  mean and variance as input. The abscissa refers to the 24-hour forecast horizon starting from the hour  $h = 9$  UTC where the observations are available, so that look-ahead time equal to 1 corresponds the forecast time at the hour  $h+1$  UTC, and so on for the other abscissa values.

to produce a forecast from observed data: the wind speed known at hour  $h$  is maintained for all considered look-ahead forecast horizons. This is thus a prediction based on persistence whose values are encoded in the variable  $O_1$  in Step 1 and 2 of our dynamic calibration with  $P = 1$ .

Let us start by emphasizing the weakness of the static calibration  $EMOS_{+4r}$  in the first forecast hours, a fact that motivated us to propose a dynamic calibration. To do that, let us imagine to have real-time data available at the hour  $h$  ( $h$  belongs to the first 24 hours from the 00 UTC) and to have at our disposal the  $EMOS_{+4r}$  static calibration starting from 00 UTC with a forecast horizons of 48 hours. The  $EMOS_{+4r}$  skill score (for both NMAE and correlation coefficient  $\mathcal{C}$ ) is reported in Fig. 10 where the abscissa refers to the 24-hour forecast horizon starting from the hour  $h$  where the observations are available (so that an abscissa equal to one corresponds to the forecast time at

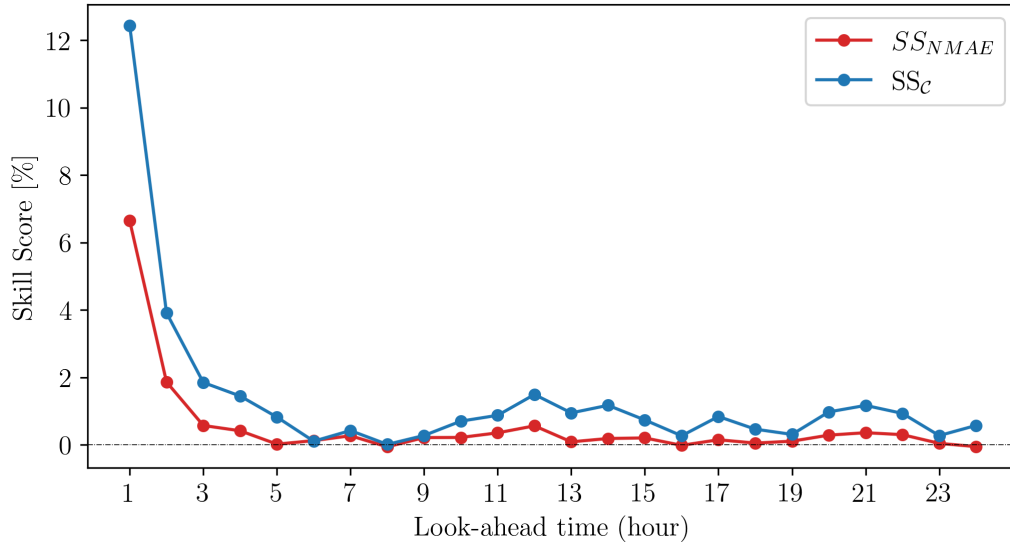


Figure 8: As in Fig. 7 but now the reference calibration is the one carried out in terms of our dynamic calibration without Step 2.

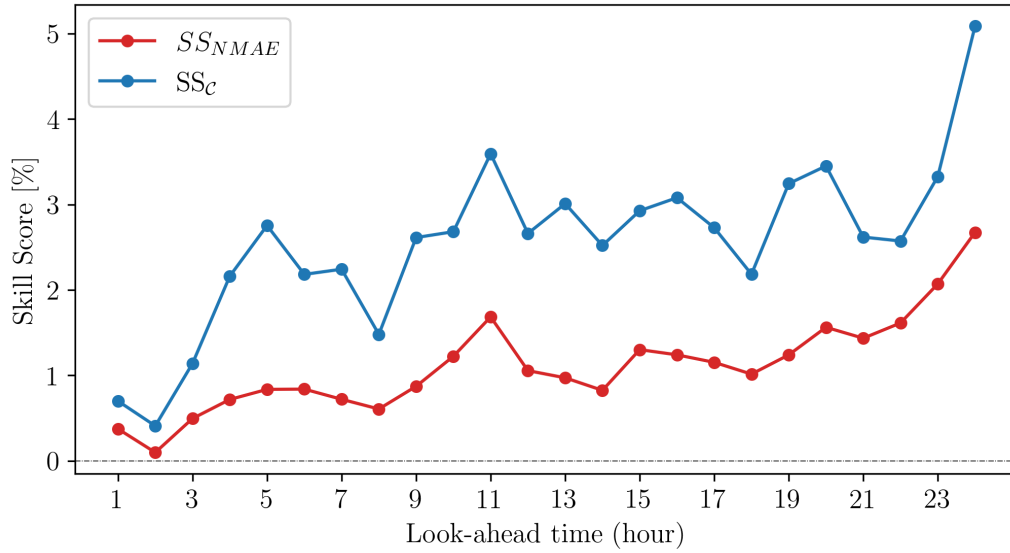


Figure 9: As in Fig. 7 but now the reference calibration is the one carried out in terms of our dynamic calibration without Step 3.

the hour  $h+1$ ). Such observation is not ingested by the static  $EMOS_{+4r}$  calibration but is used here to build a forecast based on persistence which serves as reference forecast to evaluate the  $EMOS_{+4r}$  skill score of Fig. 10. The obtained skill scores are computed averaging over all stations and over all hours  $h$  in the first 24 hours starting from 00 UTC. The shaded areas represent the 50 % confidence interval around the median thus providing us an idea on how the skill score varies among the different stations and by varying the hour  $h$  at which data are available. As one can clearly see from Fig. 10 persistence overcomes  $EMOS_{+4r}$  in the first forecast hour while rapidly deteriorating from the second hour onwards. This holds true in terms of both NMAE and correlation coefficient. The performance of our dynamic calibration is

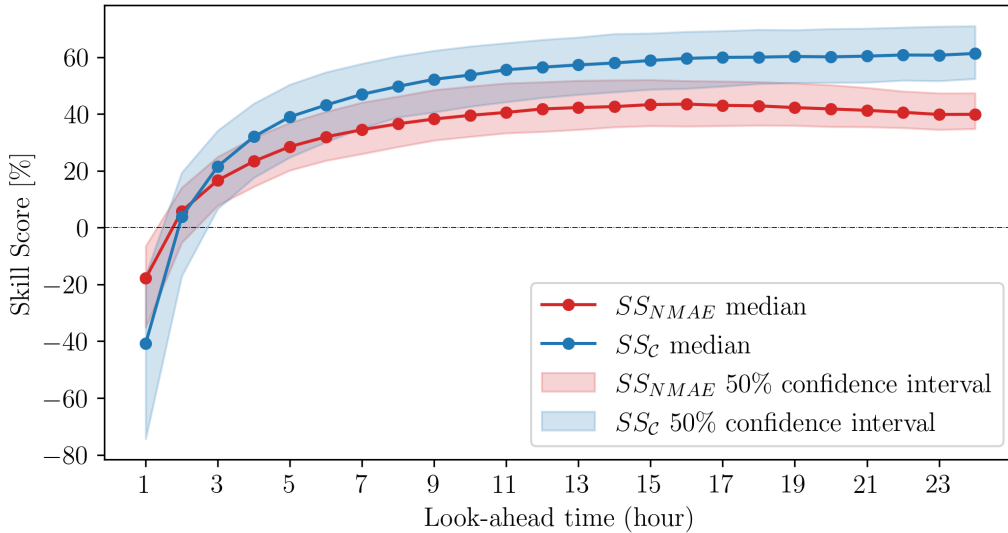


Figure 10: Skill score of NMAE and correlation coefficient of the  $EMOS_{+4r}$  static calibrated forecast using the persistence at time  $h$  as a reference forecast. Continuous lines: median of the skill scores computed by considering all stations and all hours  $h$  within the first 24 hours from 00 UTC. Shaded areas represent the 50% confidence interval of the skill scores, accounting for the variability of the latter among stations and while varying the hour  $h$  at hourly steps between 00 UTC and 24 UTC of the same day.

shown in Fig. 11 where the associated skill scores are shown by taking the persistence as a reference forecast. As one can see, our strategy overcomes persistence from the first hour onwards while maintaining the quality of the  $EMOS_{+4r}$  static calibration already detectable from Fig. 10 for sufficiently long forecast horizons. This last remark can be clearly detected from Fig. 12



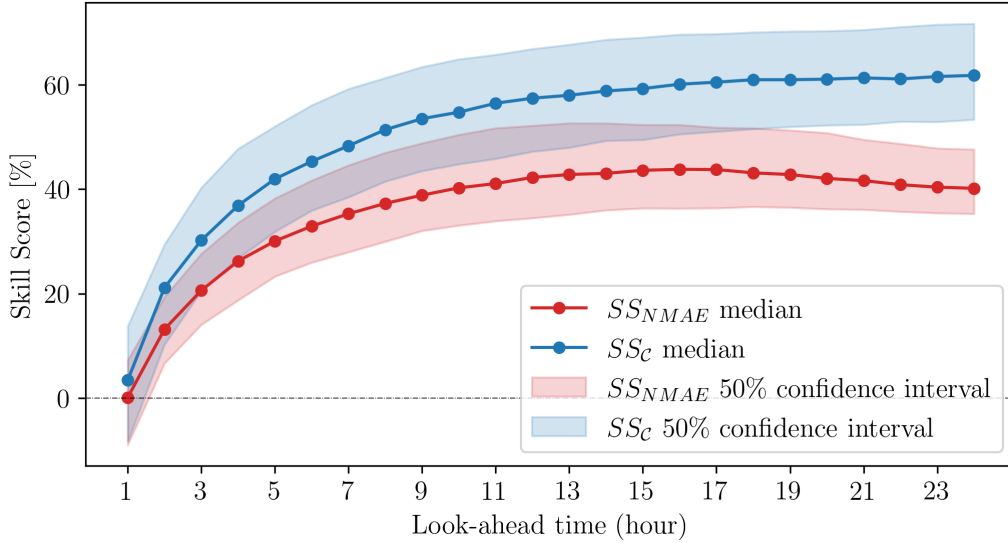


Figure 11: As in Fig. 10 but now the skill of our dynamic calibration is assessed against persistence.

where the skill score of the dynamic calibration is now presented taking the static calibration from the  $EMOS_{+4r}$  as a reference. A remarkable added value brought from the dynamic calibration clearly emerges in the first 6-7 hours, progressively reducing as the forecast horizon increases. Interestingly, the benefit carried by the ingestion of the observed data never disappears, even for the farrest look-ahead forecast times.

Let us conclude the assessment in terms of point error indices by evaluating the skill of our dynamic calibration against the prediction built from a ML-based algorithm detailed in Appendix B. This latter only uses observed data available at hour  $h = 9$  UTC with a forecast horizon of 12 hours. Results are reported in Fig. 13 and show how the dynamic calibration outperforms the observation-driven ML-based prediction.

We have till now considered point error indices. Let us now pass to assess the predictive probability density function as a whole. This is done in Fig. 14 in terms of the so-called reliability index ( $\Delta$ ) proposed by Delle Monache et al. (2006), and the sharpness  $Sh50$  corresponding to the average width of the central 50% prediction interval of a forecast probability distribution as proposed by Gneiting et al. (2007). Details are reported in Appendix A.

In Fig. 14 the reference forecast is the static  $EMOS_{+4r}$  calibration. The

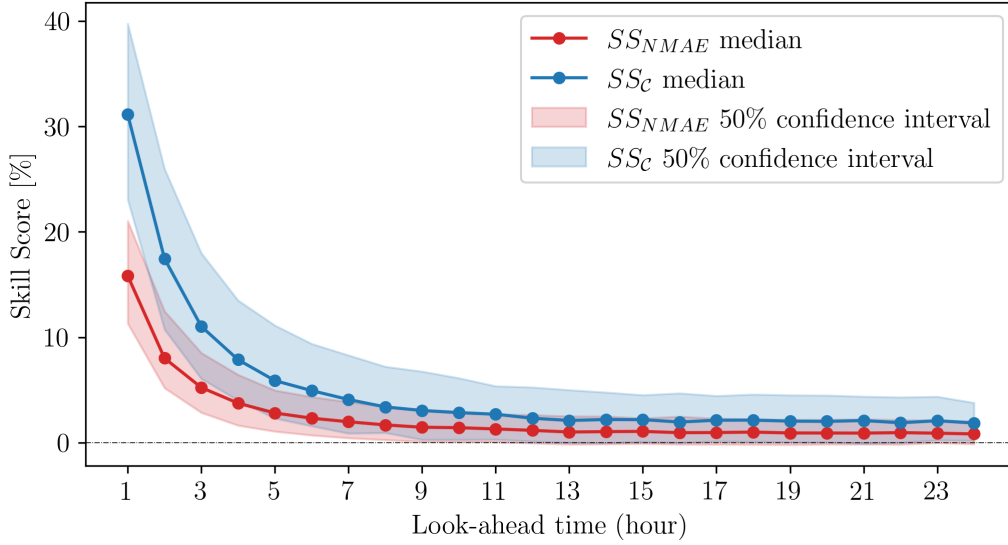


Figure 12: As in Fig. 10 but now the skill of our dynamic calibration is assessed against the static  $EMOS_{+4r}$  calibration.

increased skills of the dynamic calibration overcoming the static calibration especially in the first forecast hours is evident, thus completing our quality assessment.

A short summary of the most relevant error indices considered in the present study are reported in Tab. 4.3 for our dynamic calibration and, for comparison, for the static calibration and persistence. Results are presented for three forecast time intervals starting from the hour  $h$  at which observations are available. For the sake of example, the interval 1-2 hours means that the reported indices are the average of the corresponding indices at hours  $h+1$  and  $h+2$ . A further average is performed over all possible  $h$  between 1 and 24 hours (hourly step) and over all stations. The table confirms all conclusions drawn in the paper on the superiority of our dynamic calibration against the static one and, even more, against persistence.

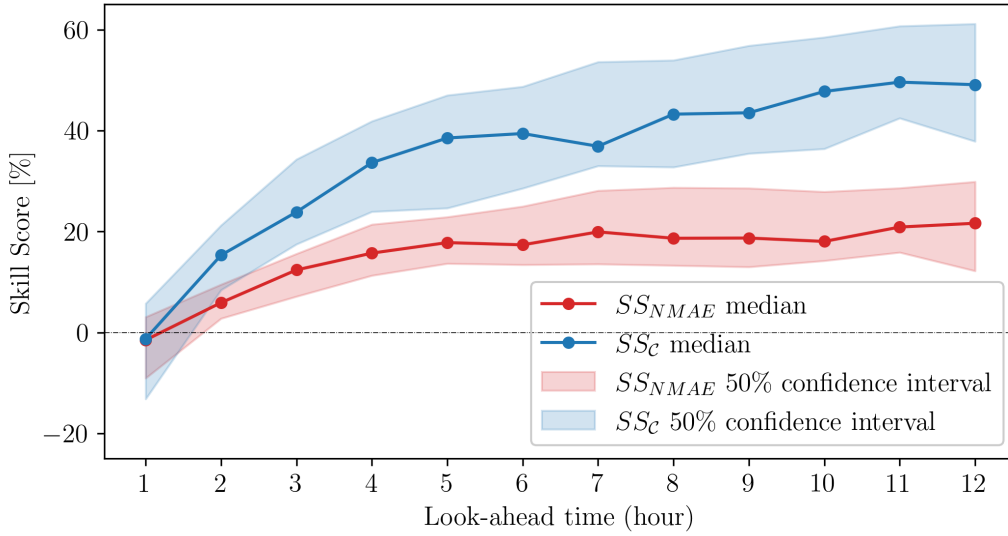


Figure 13: As in Fig. 10 but now the skill of our dynamic calibration is assessed against the ML observation-driven predictions. Also note that in this comparison we have confined the attention to the sole case corresponding to  $h = 9$  UTC with a forecast horizon of 12 hours. The 50% confidence interval thus gives us an idea on the variability of the skill score from station to station.

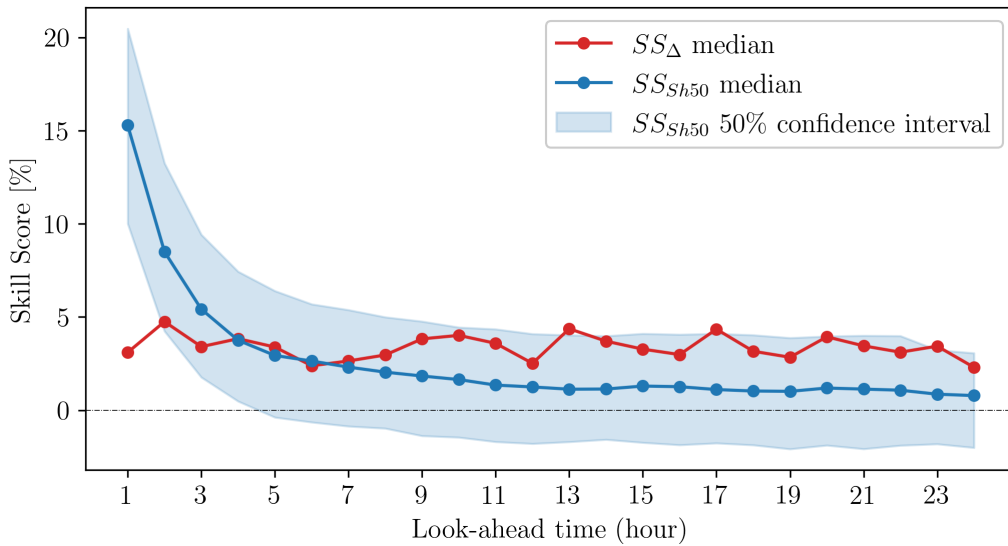


Figure 14: As in Fig. 12 but now the skill scores are computed for  $\Delta$  and the sharpness parameter  $Sh50$ . For the skill score of  $\Delta$  the confidence interval (not shown) varies between -20 and 20 %.

Table 1: A final summary of relevant indices used to assess the skill of the calibrations.

	Persistence	Static calibration	Dynamic calibration	
NMAE	0.32	0.34	0.30	1-2 h
$\mathcal{C}$	0.76	0.71	0.78	
Sh <sub>50</sub>	-	3.5	3.1	
NMAE	0.43	0.35	0.33	3-4 h
$\mathcal{C}$	0.62	0.71	0.74	
Sh <sub>50</sub>	-	3.5	3.3	
NMAE	0.51	0.35	0.34	5-6 h
$\mathcal{C}$	0.52	0.71	0.72	
Sh <sub>50</sub>	-	3.5	3.4	

## 5. Conclusions and perspectives

A novel EMOS strategy, baptized  $EMOS_{+4r}$ , has been recently proposed by Casciaro et al. (2021). This strategy differs from the standard EMOS in that the free parameters entering the predictive EMOS probability density function are categorical functions, and not constant as in the standard EMOS. This allows the introduction of nonlinearities in the calibration strategy. These categorical functions must be best-fitted for each combination of classes' levels, via a training set, by minimizing the CRPS.

If, on one hand, the new calibration strategy brings a relevant added value with respect to the standard EMOS calibration, on the other hand persistence built in terms of an observation made available at the hour  $h$  turns out to be more accurate at the next hour  $h+1$ , rapidly degrading at the next look-ahead forecast times. This simple observation suggested us that persistence could have been favorably ingested in the static  $EMOS_{+4r}$  calibration with the following two main aims: i) taking advantage of the known information from observed data at hour  $h$  in between two consecutive synoptic hours; ii) maintaining, and possibly increasing, the well-established superiority of  $EMOS_{+4r}$  over persistence after the hour  $h+1$ . Transforming this idea into a new dynamic calibration strategy taking advantage of real-time observed data has been the main result of the present paper.

At the same time, the new calibration maintains the well-established superiority of  $EMOS_{+4r}$  in the far forecast horizons over purely data-driven statistical forecasts, including complex ML-based predictions.

The higher quality of the wind speed forecast over forecasts by static approaches not ingesting real-time observations, and remaining frozen between two successive six-hour separated synoptic hours, is expected to generate a relevant added value for the wind power forecast with many useful applications for the whole wind industry.

To conclude with some perspectives, our new strategy paves the way to a myriad of other applications of interest for the green energy market. What we did for the wind speed can indeed be easily generalized to other green sources, including solar radiation and wave generation (Lira Loarca et al., 2021; Ferrari et al., 2020; Besio et al., 2016). The key ingredient for the strategy to be implemented is to have at disposal observed data in real/quasi-real time, a requirement getting easier every day.

## 6. Acknowledgments

G.C. has been funded by the Italian bank foundation “Fondazione Carige”. A.M. acknowledges the funding from the Interreg Italia-Francia Marittimo SICOMAR+ project (grant number D36C17000120006) and from the Compagnia di San Paolo (Project MINIERA No. I34I20000380007). A.L.L has been funded by the Interreg Italia-Francia Marittimo SINAPSI Project (grant number D64I18000160007). We thank the Aeronautica Militare - Servizio Meteorologico - for providing us with the SYNOP data as well as data from the EPS forecasts. Discussions with Lorenzo Rosasco, Agnese Seminara, and Alessandro Verri are warmly acknowledged.

## Appendix A. Statistical indices

The Skill Score (SS) index (Wilks, 2011) is used here to make the comparison between different calibration strategies as quantitative as possible. It assesses the performance of a given calibration by comparing its associated statistical error index against the one corresponding to a reference forecast. Namely,

$$SS = \frac{A - A_{ref}}{A_{opt} - A_{ref}} \quad (\text{A.1})$$

where  $A$  is the value of a suitable error index associated to the calibrated forecast,  $A_{ref}$  is the same as  $A$  but relative to a reference forecast. Finally,  $A_{opt}$  refers to the optimal index value. A perfect calibration yields  $SS=1$ , corresponding to the upper bound of SS. Values of SS smaller than one (including negative values) indicate that the calibrated forecast is less accurate than the reference one.

As far as the error indices are concerned ( $A$  in Eq. (A.1)), here we consider the normalized mean absolute error (NMAE), the correlation coefficient ( $\mathcal{C}$ ), the so-called reliability index ( $\Delta$ ) proposed by Delle Monache et al. (2006), and the sharpness  $Sh50$  corresponding to the average width of the central 50% prediction interval of a forecast probability distribution as proposed by Gneiting et al. (2007).

The NMAE is defined as:

$$NMAE = \frac{\sum_{n=1}^N |X_n - Y_n|}{\sum_{n=1}^N Y_n} \quad (\text{A.2})$$

where  $Y_n$  is the  $n$ -th observation and  $X_n$  is the corresponding  $n$ -th forecast (here corresponding to the mean of the 50 EPS ensemble) and  $N$  is the number of observation-forecast pairs in a given test set.

The correlation coefficient,  $\mathcal{C}$ , is a measure of linear dependence between two variables and ranges from -1 to 1, with 1 representing the highest correlation and -1 representing the highest anti-correlation (Wilks, 2011). Quantitatively (Lee Rodgers and Nicewander, 1988),

$$\mathcal{C} = \frac{\sum_{n=1}^N (X_n - \bar{X})(Y_n - \bar{Y})}{N\sigma_X\sigma_Y} \quad (\text{A.3})$$

with:

$$\sigma_X = \sqrt{\frac{\sum_{n=1}^N (X_n - \bar{X})^2}{N}} \quad (\text{A.4})$$

$$\sigma_Y = \sqrt{\frac{\sum_{n=1}^N (Y_n - \bar{Y})^2}{N}} \quad (\text{A.5})$$

where  $\bar{X}$  and  $\bar{Y}$  are the mean values of  $X$  and  $Y$ .

The goal of the probabilistic forecast, according to Gneiting et al. (2007), is to maximize the sharpness of the predictive distribution subject to calibration. Anderson (1996) and Hamill and Colucci (1997) proposed the use of verification rank (VR) histograms to assess the calibration of ensemble forecasts. VR histograms show the distribution of the ranks when the ranks of the observations are pooled within the ordered ensemble forecasts. In a calibrated ensemble, the observations and ensemble predictions should be interchangeable, resulting in a uniform VR histogram. The continuous analogue of the VR histogram is the probability integral transform (PIT) histogram (Dawid, 1984; Diebold et al., 1997; Gneiting et al., 2007). The PIT value is determined by the value of the predictive cumulative distribution function at the verifying observation. For calibrated forecasts, the empirical cumulative distribution function of PIT values should converge to the uniform distribution. The reliability index  $\Delta$  was proposed by Delle Monache et al. (2006) to quantify the deviation of VR histograms from uniformity. To quantify the deviation from uniformity in the PIT histograms, we use here the following definition of  $\Delta$ :

$$\Delta = \sum_{i=1}^m \left| f_i - \frac{1}{m} \right| \quad (\text{A.6})$$

where  $m$  is the histogram number of classes, each with a relative frequency of  $1/m$ , and  $f_i$  is the observed relative frequency in class  $i$ .

This index ranges from 0 to  $+\infty$ , with the bound zero corresponding to optimality.

Sharpness is a property of forecasts that refers to the concentration of predictive distributions. The sharper the forecasts, the more concentrated the predictive distributions are, and the sharper the better, subject to calibration.

To assess sharpness we average the widths of the central 50% prediction intervals of forecast probability distributions at all time instants. Namely,

$$Sh_P = \frac{1}{T} \sum_{t=1}^T \left[ Q \left( f(t), \frac{1}{2} + \frac{P}{2} \right) - Q \left( f(t), \frac{1}{2} - \frac{P}{2} \right) \right] \quad (\text{A.7})$$

where  $T$  is the total number of instants,  $Q$  is the quantile of the forecast distribution,  $f(t)$  is the predictive distribution at time  $t$  and  $P$  is the probability interval (here 50%).

## Appendix B. Technical Note on Machine Learning Models used as Benchmark

As a further benchmark, beside the naive Persistence Method, we use a Machine Learning approach which is based only on time series of measured data. In last years Machine Learning algorithms have been proliferating in the field of data-driven wind speed prediction, establishing itself as a competitive alternative to state-of-the-art statistical models in the field of time series forecasting in general (Parmezan et al., 2019). Here we adopt the strategy proposed in Lagomarsino Oneto et al. (2022), where wind time series are used to map the forecast task into Supervised Learning problems which they solve with a nonlinear kernel method (Bishop, 2016). In Lagomarsino Oneto et al. (2022) they find that, depending on location, direction can be useful to increase the prediction accuracy. To exploit this information they also consider the two Cartesian components of the wind vector  $u_t, v_t$  which can be easily calculated from the original signals of wind speed  $s_t$  and direction  $\theta_t$  as  $v_t = s_t \sin(\theta_t)$  and  $u_t = s_t \cos(\theta_t)$  (being the angle  $\theta_t$  measured in radians). Following their steps we define Machine Learning models which are able to learn, for each time  $t$ , the relation between the future value of the



wind speed at time  $t + h$  and the past  $\mu$  measurements (we will also refer to  $\mu$  as memory), i.e.

$$\widehat{s}_{t+h} = \mathcal{F}(\eta_{t-\mu+1}, \dots, \eta_t) \quad (\text{B.1})$$

where  $\mathcal{F}$  denotes the desired relation,  $\widehat{s}_{t+h}$  our prediction at horizon  $h$  and  $\eta_t$  the values of the input variables at time  $t$ .

Learning function  $\mathcal{F}$  can be seen as a regression problem in the context of Supervised Learning. To solve the problem, input-output couples  $(\mathbf{x}_t, y_t)_{t=1}^n$  can be defined as

$$\mathbf{x}_t = [\eta_{t-\mu+1}, \dots, \eta_t] \in \mathbb{R}^d \quad (\text{B.2})$$

$$y_t = s_{t+h} \quad (\text{B.3})$$

where  $n$  is the number of provided samples,  $d = \mu \times k$  and  $k$  is the number of variables used to define  $\eta_t$ . Denote by  $\mathbf{X} \in \mathbb{R}^{n \times d}$  (for a certain  $d$ ) the lag matrix whose rows are  $\mathbf{x}_t$  and  $\mathbf{y} \in \mathbb{R}^n$  be the vector of the outputs with elements  $y_t$ . Linear regression assumes that future wind behavior depends linearly on its past trends: it aims to find coefficients  $\boldsymbol{\beta} \in \mathbb{R}^d$  such that the following error term is minimized

$$\frac{1}{n} \sum_{i=1}^n \|\mathbf{x}_i \boldsymbol{\beta} - y_i\|^2 = \frac{1}{n} \|\mathbf{X} \boldsymbol{\beta} - \mathbf{y}\|^2 \quad (\text{B.4})$$

and hence the formula  $\mathbf{x}_{\text{new}} \boldsymbol{\beta}$  is used to infer how the wind will evolve in the future. To allow our models to capture more complex dependencies we perform Kernel Ridge Regression (KRR) introducing a non-linear transformation of the features via the kernel function  $k : \mathbb{R}^d \times \mathbb{R}^d \rightarrow \mathbb{R}$  (Murphy, 2012). In our experiments we use the Gaussian kernel which is defined as  $k(\mathbf{x}_i, \mathbf{x}_j) = e^{-\|\mathbf{x}_i - \mathbf{x}_j\|^2 / (2\sigma^2)}$ . The solution to the KRR problem yields an estimator  $\widehat{f}$  which can be used for inference

$$\widehat{f}(\mathbf{x}_{\text{new}}) = k(\mathbf{x}_{\text{new}}, \mathbf{X})(\mathbf{K} + n\lambda\mathbf{I})^{-1}\mathbf{y} \quad (\text{B.5})$$

where  $\mathbf{K} \in \mathbb{R}^{n \times n}$  is the kernel matrix with values  $\mathbf{K}_{ij} = k(\mathbf{x}_i, \mathbf{x}_j)$  and  $\lambda$  is a regularization parameter which ensures the problem is well-posed and must be tuned in order to optimize the predicting performance of the model. Since we focus on predictions delivered daily at 9:00 a.m. then only inputs vectors whose reference times  $t$  correspond to that time of day have been kept. Furthermore we aim to predict the wind speed from 1 to 12 hours ahead with

an hourly frequency and for each horizon we consider different combinations of memory  $\mu$  and input data  $\eta_t$ . We analyse all memories  $\mu$  up to 24 hours and two different cases for  $\eta_t$ . In the first case  $\eta_t = s_t$ , i.e. the input data is the wind speed itself; in the second case  $\eta_t = (u_t, v_t)$ : the two components of the wind vector, which encodes the wind speed but also the direction. A reduction of the dimension of input vectors have also been evaluated performing a Principal Component Analysis on the input samples and keeping subsets of principal components with increasing importance. Finally for each pair of horizon and location we select the setup, in terms of memory and input design (either with or without dimensionality reduction), that maximises the Pearson Correlation between predictions and actually observed values of the speed. Data from each station have been split into disjoint training and test set as described in section 3.1. Again following Lagomarsino Oneto et al. (2022) a static rather than a rolling approach is used for training. We then further split the training set to estimate model hyperparameters  $\lambda$  and  $\sigma$  using five-fold cross-validation. We performed an extensive 2-step grid-search to find the hyperparameters which minimize the  $R^2$  score for each separate location. In the first step a coarse-grained grid was used to identify the area in which hyperparameters were acceptable, in the second step we zoomed in around such area to further refine the hyperparameter values.

## References

- Abramowitz, M., Stegun, I. A., 1948. Handbook of mathematical functions with formulas, graphs, and mathematical tables. Vol. 55. US Government printing office.
- Anderson, J. L., 1996. A method for producing and evaluating probabilistic forecasts from ensemble model integrations. *Journal of Climate* 9 (7), 1518–1530.
- Baran, S., Lerch, S., 2015. Log-normal distribution based Ensemble Model Output Statistics models for probabilistic wind-speed forecasting. *Quarterly Journal of the Royal Meteorological Society* 141 (691), 2289–2299.
- Besio, G., Mentaschi, L., Mazzino, A., 2016. Wave energy resource assessment in the Mediterranean Sea on the basis of a 35-year hindcast. *Energy* 94, 50–63.

- Bishop, C. M., 2016. *Pattern Recognition and Machine Learning*. Springer New York, New York, NY, softcover reprint of the original 1st edition 2006 (corrected at 8th printing 2009) edition.
- Buizza, R., 1995. Optimal perturbation time evolution and sensitivity of ensemble prediction to perturbation amplitude. *Quarterly Journal of the Royal Meteorological Society* 121 (527), 1705–1738.
- Buizza, R., 2018. Ensemble forecasting and the need for calibration. In: *Statistical Postprocessing of Ensemble Forecasts*. Elsevier, pp. 15–48.
- Casciaro, G., Ferrari, F., Mazzino, A., 2021. Novel strategies of Ensemble Model Output Statistics (EMOS) for calibrating wind speed/power forecasts. arXiv preprint arXiv:2108.12174.
- Dawid, A. P., 1984. Present position and potential developments: Some personal views statistical theory the prequential approach. *Journal of the Royal Statistical Society: Series A (General)* 147 (2), 278–290.
- Delle Monache, L., Hacker, J. P., Zhou, Y., Deng, X., Stull, R. B., 2006. Probabilistic aspects of meteorological and ozone regional ensemble forecasts. *Journal of Geophysical Research: Atmospheres* 111 (D24).
- Diebold, F. X., Gunther, T. A., Tay, A., 1997. Evaluating density forecasts.
- Ferrari, F., Besio, G., Cassola, F., Mazzino, A., 2020. Optimized wind and wave energy resource assessment and offshore exploitability in the Mediterranean Sea. *Energy* 190, 116447.
- Glahn, H. R., Lowry, D. A., 1972. The use of model output statistics (MOS) in objective weather forecasting. *Journal of Applied Meteorology and Climatology* 11 (8), 1203–1211.
- Global Wind Energy Council, 2021. GWEC, Global Wind Report 2021, 2021-07-25.  
URL <https://gwec.net/wp-content/uploads/2021/03/GWEC-Global-Wind-Report-2021.pdf>
- Gneiting, T., Balabdaoui, F., Raftery, A. E., 2007. Probabilistic forecasts, calibration and sharpness. *Journal of the Royal Statistical Society: Series B (Statistical Methodology)* 69 (2), 243–268.

- Gneiting, T., Larson, K., Westrick, K., Genton, M. G., Aldrich, E., 2006. Calibrated probabilistic forecasting at the stateline wind energy center: The regime-switching space–time method. *Journal of the American Statistical Association* 101 (475), 968–979.
- Gneiting, T., Raftery, A. E., Westveld III, A. H., Goldman, T., 2005. Calibrated probabilistic forecasting using ensemble model output statistics and minimum CRPS estimation. *Monthly Weather Review* 133 (5), 1098–1118.
- Hamill, T. M., Colucci, S. J., 1997. Verification of Eta–RSM short-range ensemble forecasts. *Monthly Weather Review* 125 (6), 1312–1327.
- Hersbach, H., 2000. Decomposition of the continuous ranked probability score for ensemble prediction systems. *Weather and Forecasting* 15 (5), 559–570.
- ICAO, 2007. *Meteorological Service for International Air Navigation: Annex 3 to the Convention on International Civil Aviation*, 16th edn. International Civil Aviation Organization: Montreal, Canada.
- Impram, S., Nese, S. V., Oral, B., 2020. Challenges of renewable energy penetration on power system flexibility: A survey. *Energy Strategy Reviews* 31, 100539.
- Lagomarsino Oneto, D., Meanti, G., Pagliana, N., Verri, A., Mazzino, A., Rosasco, L., Seminara, A., 2022. Physics informed shallow machine learning for wind speed prediction. In preparation.
- Lee Rodgers, J., Nicewander, W. A., 1988. Thirteen ways to look at the correlation coefficient. *The American Statistician* 42 (1), 59–66.
- Leutbecher, M., Palmer, T. N., 2008. Ensemble forecasting. *Journal of Computational Physics* 227 (7), 3515–3539.
- Lira Loarca, A., Ferrari, F., Mazzino, A., Besio, G., 2021. Future wind and wave energy resources and exploitability in the Mediterranean Sea by 2100. *Applied Energy* 302, 117492.
- Molteni, F., Buizza, R., Palmer, T. N., Petroliagis, T., 1996. The ECMWF ensemble prediction system: Methodology and validation. *Quarterly Journal of the Royal Meteorological Society* 122 (529), 73–119.

- Montani, A., Gascon, E., Hewson, T., Paccagnella, T., Pilloso, F., Pincini, G., 2019. Performance of ECMWF- and COSMO-based ensemble forecast systems for precipitation events over Italy. EMS Annual Meeting Abstracts Vol. 16, EMS2019-146.
- Murphy, K. P., 2012. Machine learning: a probabilistic perspective. MIT press.
- Parmezan, A. R. S., Souza, V. M., Batista, G. E., 2019. Evaluation of statistical and machine learning models for time series prediction: Identifying the state-of-the-art and the best conditions for the use of each model. Information Sciences 484, 302–337.
- Persson, A., 2001. User guide to ECMWF forecast products. ECMWF Meteorological Bulletin M3 2.
- Scheuerer, M., Möller, D., 2015. Probabilistic wind speed forecasting on a grid based on ensemble model output statistics. The Annals of Applied Statistics 9 (3), 1328–1349.
- Soman, S. S., Zareipour, H., Malik, O., Mandal, P., 2010. A review of wind power and wind speed forecasting methods with different time horizons. In: North American Power Symposium 2010. IEEE, pp. 1–8.
- Thorarinsdottir, T. L., Gneiting, T., 2010. Probabilistic forecasts of wind speed: Ensemble model output statistics by using heteroscedastic censored regression. Journal of the Royal Statistical Society: Series A (Statistics in Society) 173 (2), 371–388.
- Wilks, D. S., 2011. Statistical methods in the atmospheric sciences. Vol. 100. Academic Press.
- Wilks, D. S., 2018. Univariate Ensemble Postprocessing. In: Statistical Post-processing of Ensemble Forecasts. Elsevier, pp. 49–84.